Adjacent Areas (California Department of Conservation, Division of Mines and Geology, Sacramento, CA, 1994); M. D. Petersen and S. G. Wesnousky, *Bull. Seismol. Soc. Am.* **84**, 1608 (1994).
4. C. DeMets, R. G. Gordon, D. F. Argus, S. Stein, *Geophys. Res. Lett.* **21**, 2191 (1994).
5. P. England and P. Molnar, *Science* **278**, 647 (1997).
6. L. M. Flesch, A. J. Haines, W. E. Holt, in preparation.
7. L. J. Sonder and C. H. Jones, *Annu. Rev. Earth Planet. Sci.* **27**, 417 (1999); B. Wernicke, *The Cordilleran Orogen; Conterminous U.S.*, vol. G-3 of *The Geology of North America*, B. C. Burchfiel, P. W. Lipman, M. L. Zoback, Eds. (Geological Society of America, Boulder, CO, 1992), pp. 553–581.
8. T. Atwater, *Geol. Soc. Am. Bull.* **81**, 3513 (1970); J. Stock and P. Molnar, *Tectonics* **7**, 1339 (1988); R. G. Bohannon and T. Parsons, *Geol. Soc. Am. Bull.* **107**, 937 (1995).
9. D. P. McKenzie, *Geophys. J. R. Astron. Soc.* **18**, 1 (1969); A. Tovish, G. Schubert, B. P. Luyendyk, *J. Geophys. Res.* **83**, 5892 (1978).
10. L. Fleitout and C. Froidevaux, *Tectonics* **1**, 21 (1982).
11. C. H. Jones, L. J. Sonder, J. R. Unruh, *Nature* **381**, 37 (1996).
12. S. Wdowinski and R. O'Connell, *J. Geophys. Res.* **96**, 12245 (1991); M. Liu and Y. Shen, *Tectonics* **17**, 311 (1998).
13. Basal tractions have a significant effect on the total stress field only if horizontal path integrals of basal tractions are of the same order of magnitude as the vertically averaged horizontal stress times the thickness of the lithosphere (10 MPa × 100 km).
14. We estimated the vertically averaged vertical stress, expressed as $\bar{\sigma}_{zz} = 1/L \int_{-h}^{L} \int_{-h}^{z} g\rho dz dz$, where ρ is the density, $h$ is the surface elevation, $L$ is an average thickness of the lithosphere, which was chosen to be 100 km here and was applied to the whole region as the scaling factor $1/L$, and $g$ is gravity (*5*, *11*). Assuming local (Airy) isostatic compensation, $\bar{\sigma}_{zz}$ was calculated assuming crustal and mantle densities of 2750 kg/m³ and 3300 kg/m³, respectively. We also used the geoid anomaly to infer GPE variations (*27*). The geoid anomaly incorporates effects of lateral density variations in both the crust and mantle and is not dependent on an assumed mechanism of compensation of topography.
15. We used the GEOID96 model (*28*) and removed terms below degree and order 7 with a cosine taper to degree and order 11 (*11*, *29*), because of a signal in the geoid from heterogeneities deep within the mantle (*30*). Following the method of (*27*), we calculated GPE estimates for the western United States using a column at sea level for reference.
16. P. England and D. P. McKenzie, *Geophys. J. R. Astron. Soc.* **70**, 295 (1982).
17. The equation of steady state motion is $\partial\sigma_{ij}/\partial x_j + \rho g \hat{z}_i = 0$, where ρ is density, $g$ is gravity, $\hat{z}_i$ is the unit vector in the $z$ direction, $\sigma_{ij}$ is total stress, and $x_j$ is the $j$th coordinate direction. We make two assumptions consistent with viscous fluid methodology: (i) that deviatoric stress can be averaged in the same fashion to the depth $L$ (100 km) as $\sigma_{zz}$ (*14*) and (ii) that tractions at the base of the lithosphere are negligible. Making these two assumptions, the horizontal-component force-balance equations condense to $\partial/\partial x_\beta(\bar{\tau}_{\alpha\beta} + \delta_{\alpha\beta}\bar{\tau}_{\gamma\gamma}) = -(\partial\bar{\sigma}_{zz}/\partial x_\alpha)$, where $\bar{\tau}_{\gamma\gamma} = \bar{\tau}_{xx} + \bar{\tau}_{yy} = -\bar{\tau}_{zz}$, $x_\alpha$ is the α coordinate direction, $\bar{\tau}_{\alpha\beta}$ is the deviatoric stress tensor, $\delta_{\alpha\beta}$ is the Krunecker delta function, and $\bar{\sigma}_{zz}$ is the vertically averaged vertical stress (potential energy), which is used as input (*6*).
18. We used the variational principle (*31*) to minimize the functional $I = \int_S [\bar{\tau}_{\alpha\beta}\bar{\tau}_{\alpha\beta} + (\bar{\tau}_{\gamma\gamma})^2] dS + \int_S 2\lambda_\alpha [(\partial/\partial x_\beta)(\bar{\tau}_{\alpha\beta} + \delta_{\alpha\beta}\bar{\tau}_{\gamma\gamma}) + (\partial\bar{\sigma}_{zz}/\partial x_\alpha)] dS$ with respect to $\bar{\tau}_{\alpha\beta}$, where $S$ is the area of Earth's surface being considered and $\lambda_\alpha$ is the Lagrange multiplier for the differential equation constraint (*17*), which yields the requirements that $\bar{\tau}_{\alpha\beta} = 1/2[(\partial\lambda_\alpha/\partial x_\beta) + (\partial\lambda_\beta/\partial x_\alpha)]$ and the vector $\lambda_\alpha = 0$ everywhere on $\partial S$. Again using the variational principle, minimization of the functional

$$J = \int_S \left[ 2\left(\bar{\tau}_{xx} + \frac{1}{3}\bar{\sigma}_{zz}\right)^2 + 2\left(\bar{\tau}_{xx} + \frac{1}{3}\bar{\sigma}_{zz}\right) \times \left(\bar{\tau}_{yy} + \frac{1}{3}\bar{\sigma}_{zz}\right) + 2\left(\bar{\tau}_{yy} + \frac{1}{3}\bar{\sigma}_{zz}\right)^2 + 2\,\bar{\tau}_{xy}^2 \right] dS$$

with respect to $\lambda_\alpha$ provides a self-consistent solution to the force-balance equations (*17*). These expressions were for the flat-Earth approximation, but we were actually using the corresponding expressions for the spherical Earth (*6*), which have the same structure but less simple forms.
19. In isotropic media, stress, $\bar{\tau}_{\alpha\beta}$, and strain rate, $\dot{\varepsilon}_{\alpha\beta}$, are related by $\bar{\tau}_{\alpha\beta} = \bar{\eta}\dot{\varepsilon}_{\alpha\beta}$, where $\bar{\eta}$ is the effective viscosity for a power law fluid rheology (*16*).
20. We solved for three stress field basis functions, defined by three separate sets of Lagrange multiplier values, $\Lambda_i = (\lambda_\alpha, \lambda_\beta)$, assigned to the PA Plate boundary and applied in the functionals $I$ and $J$ (*18*). Minimization of functional $J$ (*18*) again satisfies force-balance equations (*17*) with $\bar{\sigma}_{zz}$ now set to zero in the functionals. The assigned values for $\Lambda_i$ define the specific stress field boundary conditions for the three stress field basis functions and were the three most spatially uniform cases $\Lambda_i = \omega_i \times r$, where $r$ marks the radial position vector along the PA Plate boundary and $\omega_i$ are three orthogonal rotation vectors (0°N, 0°E, 1), (0°N, 90°E, 1), and (90°N, 0°E, 1). A linear combination of the three stress field basis functions (Fig. 2B), added to the deviatoric stresses associated with GPE variations (Fig. 2A), defined the total stress field (Fig. 2C). The coefficients of the three basis functions in this linear combination are found by iterative least squares inversion for the best fit between the tensor styles of the resulting total stress field and the styles inferred from stress indicators (*2*) [that is, the styles of the strain rates inferred from GPS and VLBI data (*1*), Quaternary fault data (*3*), and imposed NUVEL-1A plate motion (*4*)] (*6*).
21. M. D. Zoback *et al.*, *Science* **238**, 1105 (1987); V. S. Mount and J. Suppe, *Geology* **15**, 1143 (1987); A. H. Lachenbruch and J. H. Sass, *J. Geophys. Res.* **97**, 4995 (1992); M. L. Zoback, *J. Geophys. Res.* **94**, 7105 (1989); M. L. Zoback, *J. Geophys. Res.* **97**, 11703 (1992).
22. L. E. Gilbert, C. H. Scholz, J. Beavan, *J. Geophys. Res.* **99**, 23975 (1994).
23. Because the force-balance equations in (*17*) are linear in stress, any number of solutions can be superimposed. This is true even for power law rheology. Stresses resulting from individual tectonic sources (boundary forces) and internal buoyancy effects (body forces) can be added linearly. What does not add linearly with a power law rheology is strain rate.
24. E. D. Humphreys and K. G. Duker, *J. Geophys. Res.* **99**, 9635 (1994); M. Liu and Y. Shen, *Geology* **26**, 299 (1998).
25. B. G. Bills, D. R. Currey, G. A. Marshall, *J. Geophys. Res.* **99**, 22059 (1994); B. G. Bills, K. D. Adams, S. G. Wesnousky, *Eos* **76**, 608 (1995); J. Deng, M. Gurnis, H. Kanamori, E. Hauksson, *Science* **282**, 1689 (1998); F. F. Pollitz, G. Peltzer, R. Burgmann, *Eos* **79**, F601 (1998).
26. A. J. Haines and W. E. Holt, *J. Geophys. Res.* **98**, 12057 (1993).
27. D. D. Coblentz, R. M. Richardson, M. Sandiford, *Tectonics* **13**, 929 (1994).
28. D. A. Smith and D. G. Milbert, *J. Geodesy* **73**, 219 (1999).
29. A. F. Sheehan and S. C. Solomon, *J. Geophys. Res.* **96**, 19981 (1991).
30. B. H. Hager, R. W. Clayton, M. A. Richards, R. P. Comer, A. M. Dziewonski, *Nature* **331**, 541 (1985).
31. P. M. Morse and H. Feshbach, in *Methods of Theoretical Physics* (McGraw-Hill, New York, 1953), pp. 275–347.
32. The San Andreas fault may be weak in the direction of slip (*22*) and therefore rheologically anisotropic. When we assigned the strain rates from the kinematic solution (*2*) to the 12 areas containing the San Andreas fault, we obtained the full PA-NA Plate motion.
33. We thank W. Thatcher and his group for allowing us use of their GPS data before publication, C. Jones for sharing the geoid filtering code, and two anonymous reviewers. Maps were prepared with GMT version 3.0 by P. Wessel and W.F. Smith. This work was supported by an NSF career grant to W.E.H. (EAR- 962 8872) and U.S. Geological Survey grant 99HQGR0010. A.J.H.'s contribution has been supported by the Marsden Fund administered by the Royal Society of New Zealand.

22 September 1999; accepted 6 December 1999

# High-Speed Electrically Actuated Elastomers with Strain Greater Than 100%

**Ron Pelrine,* Roy Kornbluh, Qibing Pei, Jose Joseph**

**Electrical actuators were made from films of dielectric elastomers (such as silicones) coated on both sides with compliant electrode material. When voltage was applied, the resulting electrostatic forces compressed the film in thickness and expanded it in area, producing strains up to 30 to 40%. It is now shown that prestraining the film further improves the performance of these devices. Actuated strains up to 117% were demonstrated with silicone elastomers, and up to 215% with acrylic elastomers using biaxially and uniaxially prestrained films. The strain, pressure, and response time of silicone exceeded those of natural muscle; specific energy densities greatly exceeded those of other field-actuated materials. Because the actuation mechanism is faster than in other high-strain electroactive polymers, this technology may be suitable for diverse applications.**

New high-performance actuator materials capable of converting electrical energy to mechanical energy are needed for a wide range of demanding applications, such as mini- and microrobots, micro air vehicles, disk drives, flat-panel loudspeakers, and prosthetic devices. Many types of candidate materials are under investigation, including single-crystal piezoelectric ceramics (*1*) and carbon nanotubes (*2*). Electroactive polymers are of particular interest because of the low cost of materials and the

SRI International, 333 Ravenswood Avenue, Menlo Park, CA 94025, USA.

*To whom correspondence should be addressed. E-mail: pelrine@erg.sri.com

ability of polymers to be tailored to particular applications. Within the general category of electroactive polymers, many different types are under investigation, including electrostrictive polymers (*3, 4*), piezoelectric polymers (*5*), and electrochemically actuated conducting polymers and gels (*6–11*). Most electroactive polymers excel in some measures of performance (such as energy density or strain) but are unsatisfactory in others (such as efficiency and speed of response).

It has been well known for many years that the electric field pressure from free charges on the surface of all insulating materials induces stresses (Maxwell's stress) that strain the material. Zhenyi *et al.* (*4*) showed that a largely noncrystalline polymer (polyurethane) could produce actuated strains of 3 to 4% using metal electrodes such as 20-nm-thick gold; they estimated that 10% of their observed strain response was due to Maxwell stress. More recently, it has been suggested that Maxwell stress by itself can produce powerful electroactive responses in certain elastomers (*12, 13*). This mechanism of actuation (Fig. 1) distinguishes dielectric elastomers from most electrostrictive polymers previously reported. A dielectric elastomer film, typically 10 to 200 μm thick, is coated on each side with a compliant electrode material (e.g., carbon-impregnated grease). When a voltage is applied across the two electrodes, the electrostatic forces compress and stretch the film. Compression of the film thickness brings opposite charges closer together, whereas planar stretching of the film spreads out or separates similar charges. Both changes convert electrical energy to mechanical energy and provide the actuation mechanism.

The actuation mechanism illustrated in Fig. 1 was previously shown to have high actuation pressures (0.1 to 2 MPa), fast response times (<1 ms), and potentially high efficiencies (>80 to 90%) (*12*). A variety of elastomer materials have been investigated, including silicones such as NuSil Technology's CF19-2186 and Dow Corning's HS3. Peak strains of 32% (CF19-2186) and 41% (HS3) were demonstrated, with specific elastic energy densities up to 0.15 J/g for CF19-2186 (*12*).

We have now conducted experiments that demonstrate extraordinarily high strains, five to six times those previously reported, with higher pressures (up to 7 MPa) and energy densities about 23 times those described earlier. The improvement is due to the identification of a new dielectric actuator material (3M's VHB 4910 acrylic) as well as the application of high prestrain in one planar direction, which enhances electrical breakdown strength and causes the material to actuate primarily in the low-prestrain planar direction. We also present data on applying higher prestrains to improve the performance of previously described silicones. Higher strains and actuation pressures can potentially be exploited to improve a wide range of existing actuator devices (e.g., pumps, motors, robot actuators, generators, and flat-panel loudspeakers) as well as enable new applications (e.g., small flapping-wing vehicles, lifelike prosthetics, noise suppression devices, and biologically inspired robots).

The compression and stretching modes of actuation are mechanically coupled for most elastomers because, at the stresses of interest, the elastomer volume is essentially fixed (the bulk modulus is much higher than the modulus of elasticity $Y$). We can use our electrostatic model to show that the effective compressive stress, $p$, compressing the film in thickness (*13*) is

$$p = \varepsilon\varepsilon_o E^2 \quad (1)$$

where $\varepsilon$ is the relative dielectric constant of the material, $\varepsilon_o$ is the permittivity of free space ($8.85 \times 10^{-12}$ F/m), and $E$ is the electric field (volts per meter). The effective compressive stress in Eq. 1 is twice the stress normally calculated for two rigid, charged capacitor plates, because in an elastomer the planar stretching is coupled to the thickness compression. We refer to the stress in Eq. 1 as an effective stress because, strictly speaking, it is the result of both compressive stress acting in the thickness direction and tensile stresses acting in the planar directions. The compressive and tensile stresses are mechanically equivalent in a thin film to a single compressive stress acting in the thickness direction according to Eq. 1.

For low strains (e.g., <20%), the thickness strain $s_z$ can be approximated by

$$s_z = -p/Y = -\varepsilon\varepsilon_o E^2/Y \quad (2)$$

For strains greater than about 20%, Eq. 2 is unsatisfactory because $Y$ generally depends on the strain itself. The high actuated strains we observed require the modification of other conventional actuator material constitutive relations as well, even with an assumption of constant modulus. For example, the elastic strain energy density in an actuator material, $u_e$ (a common parameter for comparing the output capabilities of actuator materials), is typically expressed as $u_e = \frac{1}{2}ps_z = \frac{1}{2}Ys_z^2$, but this formula assumes low strains. For high strains, the planar area over which the compression acts increases substantially as the material is compressed (*12*). For high-strain, nonlinear materials, where the compressive stress is known, a more useful measure of performance might be the electromechanical energy density $e$, which we define as the amount of electrical energy converted to mechanical energy per unit volume of material for one cycle. The electromechanical energy density can be written as

$$e = -p \ln(1 + s_z) \quad (3)$$

(*14*), where $p$ is the constant compressive stress. If we substitute $p = Ys_z$ on the right side of Eq. 3 and expand the logarithm for small $s_z$, it follows that $\frac{1}{2}e = u_e$, thus providing a valid comparison between the high-strain, nonlinear materials discussed here and conventional low-strain energy density formulas for materials such as piezoelectrics.

We tested many types of polymeric elastomer films. Here we focus on three promising types: Dow Corning HS3 silicone, NuSil CF19-2186 silicone, and the 3M VHB 4910 acrylic adhesive system (*15*). As noted above, results for the silicone films were reported in earlier publications, but new high-prestrain results using these polymers are reported here.

Strain measurements were made with elastomer films stretched on a rigid frame. Compliant electrodes were stenciled with conductive carbon grease (Chemtronics Circuit Works CW7200) on the top and bottom of the films. The active, electroded portion of the stretched film was small relative to the film's total area. Thus, the inactive portions of the film acted as a spring force on the boundaries of the active regions. When a voltage difference was applied between the top and bottom electrodes, the active region expanded while the inactive region contracted. Removing the applied voltages caused the reverse change. A digital video optical system was used to measure the actuated strain. Measurements were taken about 1 s after application of the voltage. The stretched film technique for measuring strains introduces some boundary constraints from the inactive portion of the film, but it circumvents the difficulty of trying to achieve free-boundary conditions with a soft flexible material (*12*).

For an elastomer, the absolute strain under actuation depends on the prestrain. A more useful quantity is the relative strain under actuation:

$$\frac{\text{(actuated length)} - \text{(unactuated length)}}{\text{(unactuated length)}}$$

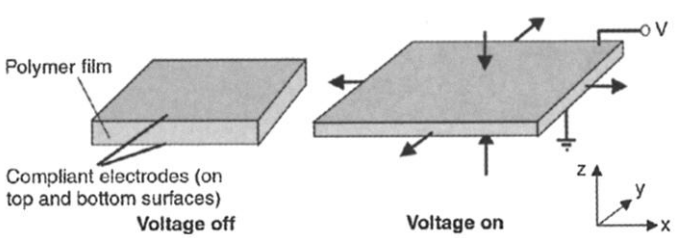


**Fig. 1.** The dielectric elastomers actuate by means of electrostatic forces applied via compliant electrodes on the elastomer film.

The relative strain equals the absolute strain if there is zero prestrain in the film. The relative area strain is defined similarly, with the active planar area replacing length in the above expression.

Two types of strain tests were performed, circular (biaxial) and linear (uniaxial). In the circular tests, a small circular active region (5 mm in diameter) was used to decrease the likelihood of a fabrication defect causing an abnormally low breakdown voltage. The film was stretched uniformly on the frame, and the circle expanded in area when a voltage was applied (Fig. 2). The expansion of the circle is equal in both $x$ and $y$ planar directions because there is no preferred planar direction for the film. By contrast, the linear strain tests used a high prestrain in one planar direction and little or no prestrain in the other planar direction. High prestrain effectively stiffens the film in the high-prestrain planar direction, which causes the film to actuate primarily in the softer, low-prestrain planar direction and in thickness. Figure 3 shows a linear strain test. The relative strain was measured in the central region of the elongated (black) active area, away from the edge constraints.

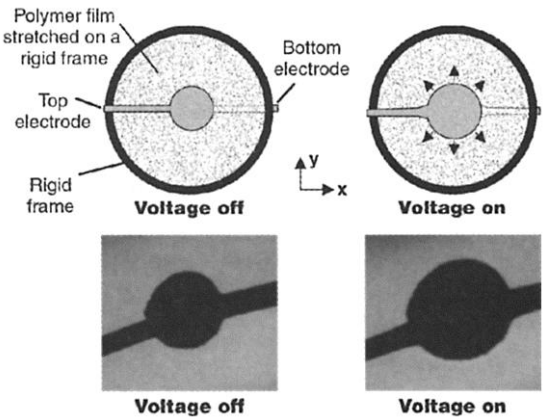


**Fig. 2.** The circular strain test measures the expansion of an actuated circle on a larger stretched film. The photo shows 68% area expansion during actuation of a silicone film.

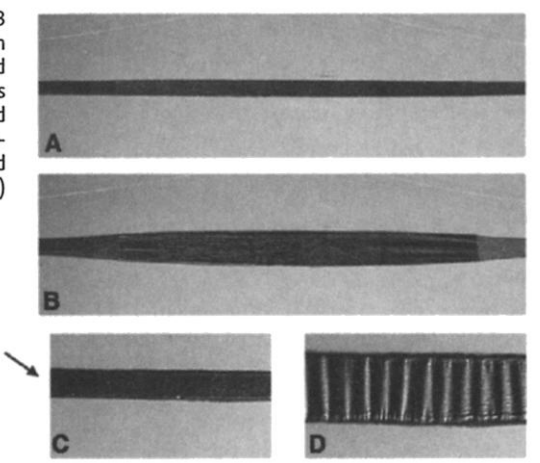


**Fig. 3.** (**A** and **B**) Linear strain test of HS3 silicone film with a high horizontal prestrain for the field off (A) and on (B) with a field of 128 V/μm; 117% relative strain was observed in the central region of (B). (**C** and **D**) Activation of acrylic elastomers, producing about 160% relative strain, for the field off (C) and on (D); the dark area in (C) indicates the active region.

The circular test results for three elastomers under different conditions of prestrain are given in Table 1. The peak relative area strain was measured directly, and the relative thickness strain was calculated from the constant volume constraint. The breakdown field was calculated from the known voltage and the measured film thickness (corrected for the given relative thickness strain). No attempt was made to minimize voltage with these relatively thick films, and voltages were typically 4 to 6 kV. Thinner films generally yield lower but comparable performance at lower voltage. For example, preliminary measurements showed 104% relative area strain at 980 V using a thinner acrylic film. The electromechanical energy density $e$ was estimated from the peak field strength (Eq. 1) and the relative thickness strain. The value $\frac{1}{2}e$ is listed in Table 1 for convenient comparison to conventional elastic energy densities available for other actuator materials.

As indicated by the values, the VHB 4910 acrylic elastomer gave the highest performance in terms of strain and actuation pressure. Extensive lifetime tests have not been made, but acrylic films have been operated continuously for several hours at the 100% relative area strain level with no apparent degradation in relative strain performance. However, the acrylic elastomer has relatively high viscoelastic losses that limit its half-strain bandwidth (the frequency at which the strain is one-half of the 1-Hz response) to about 30 to 40 Hz in the circular strain test. By comparison, HS3 silicone has been used for prototype loudspeakers at frequencies as high as 2 to 20 kHz (*16, 17*). The actuation of CF19-2186 silicone, albeit at lower strains and fields than reported here, has been measured directly via laser reflections with full strain response up to 170 Hz (resonance effects prevented measurement at higher speeds) (*12*). The only apparent fundamental limits on actuation speed are the viscoelastic losses, the speed of sound in the material, and the time to charge the capacitance of the film (electrical response time).

The strains in the linear strain test can be quite large, up to 215% for the VHB 4910 acrylic adhesive (Table 1). The VHB 4910 acrylic elastomer, when undergoing ~160% strain in a linear strain test, exhibited buckling (the vertical wrinkles in Fig. 3D) that was not seen in properly stretched silicone films. Buckling indicates that the film is no longer in tension in the horizontal direction during actuation, and that the overall relative thickness strain is greater than indicated by measurements of the electrode boundaries. That is, the relative strain numbers for VHB 4910 in Table 1 may be undervalued.

The dielectric elastomer films presented here appear promising as actuator materials

**Table 1.** Circular and linear strain test results.

| Material | Prestrain ($x$,$y$) (%) | Actuated relative thickness strain (%) | Actuated relative area strain (%) | Field strength (MV/m) | Effective compressive stress (MPa) | Estimated $\frac{1}{2}e$ (MJ/m$^3$) |
|---|---|---|---|---|---|---|
| | | | *Circular strain* | | | |
| HS3 silicone | (68,68) | 48 | 93 | 110 | 0.3 | 0.098 |
| | (14,14) | 41 | 69 | 72 | 0.13 | 0.034 |
| CF19-2186 silicone | (45,45) | 39 | 64 | 350 | 3.0 | 0.75 |
| | (15,15) | 25 | 33 | 160 | 0.6 | 0.091 |
| VHB 4910 acrylic | (300,300) | 61 | 158 | 412 | 7.2 | 3.4 |
| | (15,15) | 29 | 40 | 55 | 0.13 | 0.022 |
| | | | *Linear strain* | | | |
| HS3 | (280,0) | 54 | 117 | 128 | 0.4 | 0.16 |
| CF19-2186 | (100,0) | 39 | 63 | 181 | 0.8 | 0.2 |
| VHB 4910 | (540,75) | 68 | 215 | 239 | 2.4 | 1.36 |

because their overall performance can be good. The available literature indicates that the actuated strains of silicone are greater than for any known high-speed electrically actuated material (that is, a bandwidth above 100 Hz). Silicone elastomers also have other desirable material properties such as good actuation pressures and high theoretical efficiencies (80 to 90%) because of the elastomers' low viscoelastic losses and low electrical leakage (*12*).

The VHB 4910 acrylic adhesive appears to be a highly energetic material. The energy density of the acrylic adhesive is three times that reported for single-crystal lead–zinc niobate/lead titanate (PZN-PT) piezoelectric (about 1 MJ/m$^3$) (*1*), itself an energetic new material with performance much greater than that of conventional piezoelectrics. The density of both the silicones and the acrylic adhesive is approximately that of water and about one-seventh that of ceramic piezoelectric materials. Hence, the energy density of the acrylic adhesive on a per-weight basis (the specific energy density) is about 21 times that of single-crystal piezoelectrics and more than two orders of magnitude greater than that of most commercial actuator materials.

Potential applications for dielectric elastomer actuators include robotics, artificial muscle, loudspeakers, solid-state linear actuators, and any application for which high-performance actuation is needed. A variety of actuator devices have been made with the silicone elastomers, including rolled actuators, tube actuators, unimorphs, bimorphs, and diaphragm actuators (*12, 18, 19*). Their performance is promising, but most of this work did not exploit the benefits of high prestrain or the new acrylic material. We have built an actuator using 2.6 g of stretched acrylic film that demonstrated a force of 29 N and displacement of 0.035 m, a high mechanical output for such a small film mass. The very high strains recently achieved suggest novel applications for shape-changing devices, and the specific energy density of the acrylic adhesive is so high that, if it could be realized in a practical device, it could replace hydraulic systems at a fraction of their weight and complexity. However, practical applications require that a number of other issues be addressed, such as high-voltage, high-efficiency driver circuits, fault-tolerant electrodes, long-term reliability, environmental tolerances, and optimal actuator designs.

**References and Notes**


1. S. Park and T. Shrout, *J. Appl. Phys.* **82**, 1804 (1997).
2. R. H. Baughman *et al.*, *Science* **284**, 1340 (1999).
3. Q. M. Zhang, V. Bharti, X. Zhao, *Science* **280**, 2101 (1998).
4. M. Zhenyi *et al.*, *J. Polym. Sci. B Polym. Phys.* **32**, 2721 (1994).
5. T. Furukawa and N. Seo, *Jpn. J. Appl. Phys.* **29**, 675 (1990).
6. E. Smela, O. Inganäs, I. Lundström, *Science* **268**, 1735 (1995).
7. E. Smela and N. Gadegaard, *Adv. Mater.* **11**, 953 (1999).
8. T. Otero *et al.*, *Proc. SPIE* **3669**, 98 (1999).
9. H. B. Schreyer *et al.*, *Proc. SPIE* **3669**, 192 (1999).
10. K. Oguro *et al.*, *J. Micromachine Soc.* **5**, 27 (1992).
11. H. Tamagawa *et al.*, *Proc. SPIE* **3669**, 254 (1999).
12. R. Kornbluh *et al.*, *Proc. SPIE* **3669**, 149 (1999).
13. R. Pelrine *et al.*, *Sensors Actuators A Phys.* **64**, 77 (1998).

14. For a constant-volume material, $(1 + s_x)(1 + s_y)(1 + s_z) = 1$, where $s_x$ and $s_y$ are the length and width strains. As the film is squeezed, the area of compression $A(s_z)$ can be expressed as $A(s_z) = xy = x_o(1 + s_x)y_o(1 + s_y) = (x_o y_o z_o)/[z_o(1 + s_z)]$, where $x_o$, $y_o$, and $z_o$ are the initial length, width, and thickness of the active area of the film. The energy density converted to mechanical work is then the integral, over the displacement, of the compressive stress times the area of compression divided by the volume:

$$e = -(1/x_o y_o z_o)\int p A(s_z)dz$$

$$= -\int p[1/(1 + s_z)]ds_z = -p \ln(1 + s_z)$$

where $p$ is the assumed constant compressive stress. The minus sign is introduced because we are defining $p$ as a positive number for compression ($dz$ is negative over the integration). The assumption of constant $p$ depends on the electronic driving circuitry, which ideally would adjust the applied voltage according to the varying thickness to hold the electric field constant. It can be shown that with a nonideal, constant-voltage drive, the term $\ln(1 + s_z)$ would be replaced by $-(s_z + 0.5s_z^2)$. However, because the present focus is on the fundamental material performance rather than electronic performance, we make the simplest physical assumption that $p$ is constant.


15. The silicone films are based on a polydimethyl siloxane backbone. They were diluted in naphtha solvent, spin-coated, cured, and released. The HS3 silicone was centrifuged to remove pigment particles before spin coating. VHB 4910 is available in film form with a removable liner backing. The acrylic elastomer is made of mixtures of aliphatic acrylate photocured during film processing. Its elasticity results from the combination of the soft, branched aliphatic groups and the light cross-linking of the acrylic polymer chains. The zero-strain thicknesses of the materials were typically 225 μm for HS3, 50 μm for CF19-2186, and 1000 μm for the VHB 4910 acrylic. The relative dielectric constant at 1 kHz is 2.8 for the two silicones and was measured at 4.8 ± 0.5 for the VHB 4910 acrylic.
16. R. Heydt *et al.*, *J. Sound Vibr.* **215**, 297 (1998).
17. R. Heydt *et al.*, *J. Acoust. Soc. Am.*, in press.
18. R. Kornbluh *et al.*, *Proceedings of the Third IASTED International Conference on Robotics and Manufacturing*, Cancun, Mexico, 14 to 16 June 1995 (ACTA Press, Calgary, Alberta, 1995), pp. 1–6.
19. R. Kornbluh *et al.*, *Proceedings of the 1998 IEEE International Conference on Robotics and Automation*, Leuven, Belgium, May 1998 (IEEE Press, Piscataway, NJ, 1998), pp. 2147–2154.


20. Much of this work was performed under the management of the Micromachine Center at the Industrial Science and Technology Frontier Program, Research and Development of Micromachine Technology of MITI (Japan), supported by the New Energy and Industrial Technology Development Organization.

7 September 1999; accepted 6 December 1999


# Two-Dimensional Electronic Excitations in Self-Assembled Conjugated Polymer Nanocrystals


**R. Österbacka,* C. P. An, X. M. Jiang, Z. V. Vardeny†**



**Several spectroscopic methods were applied to study the characteristic properties of the electronic excitations in thin films of regioregular and regiorandom polythiophene polymers. In the regioregular polymers, which form two-dimensional lamellar structures, increased interchain coupling strongly influences the traditional one-dimensional electronic properties of the polymer chains. The photogenerated charge excitations (polarons) show two-dimensional delocalization that results in a relatively small polaronic energy, multiple absorption bands in the gap where the lowest energy band becomes dominant, and associated infrared active vibrations with reverse absorption bands caused by electron-vibration interferences. The relatively weak absorption bands of the delocalized polaron in the visible and near-infrared spectral ranges may help to achieve laser action in nanocrystalline polymer devices using current injection.**


Self-assembled organic semiconductor polymers with supramolecular two-dimensional (2D) structures are of interest (*1–11*) because the traditional one-dimensional (1D) electronic properties of the π-conjugated polymer chains can be modified by the increased interchain coupling. The regioregular (RR)-substituted polythiophene polymers (*7*) such as poly(3-alkylthiophene) (P3AT), in which the alkyl side groups are attached to the third position of the thiophene rings in a head-to-tail stereoregular order (Fig. 1A), form thin films with nanocrystalline lamellae (*6*), resulting in relatively high hole mobilities of 0.1 cm$^2$ V$^{-1}$ s$^{-1}$ (*8–11*).


Physics Department, University of Utah, Salt Lake City, UT 84112, USA.

*On leave from the Department of Physics and the Graduate School of Materials Research, Åbo Akademi University, Porthansgatan 3, FIN-20500 Turku, Finland.

†To whom correspondence should be addressed. E-mail: val@physics.utah.edu